Parity-based mirror inversion for efficient quantum state transfer and computation in nearest-neighbor arrays

P. Kumar* and S. Daraeizadeh
Department of Electrical and Computer Engineering, Wichita State University, Wichita, Kansas 67260, USA
(Received 10 January 2015; published 9 April 2015)

We introduce an efficient scheme for quantum state transfer that uses a parity-based mirror inversion technique. We design efficient circuits for implementing mirror inversion in Ising $\sigma_X\sigma_X$ and $\sigma_Y\sigma_Y$ coupled systems and show how to analytically solve for system parameters to implement the operation in these systems. The key feature of our scheme is a three-qubit parity gate, which we design as a two-control one-target qubit gate. The parity gate operation is implemented by only varying a single control parameter of the system Hamiltonian and the difficulty of implementing this gate is equivalent to that of a controlled-NOT gate in a two-qubit system. By applying a sequence of $N + 1$ parity-based controlled-unitary operations between nearest-neighbor qubits, where all qubits in an N-qubit chain function either as controls or targets, we are able to reverse the order of all qubits along the array. These operations are accomplished by varying only a single control parameter per data qubit. The control parameter depends on the physical system under consideration and on the choice of the designer. Since every qubit participates in the mirror-inversion process functioning either as a control or target, all nearest-neighbor couplings are used. Therefore, we do not need additional measures to cancel the effect of any unwanted interactions and the quantum cost of our scheme does not increase in systems that do not have the ability shut off couplings. Moreover, our scheme does not require additional ancillas, nor does it use a pre-engineered mirror-periodic Hamiltonian to govern the evolution of the system. Using our mirror inversion scheme, we also show how to implement a SWAP gate between two arbitrary remote qubits, move a block of qubits, and implement efficient computing between two remote qubits in nearest-neighbor layouts.

DOI: 10.1103/PhysRevA.91.042310 PACS number(s): 03.67.Hk, 03.67.Lx, 03.67.Ac

I. INTRODUCTION

Many proposed implementations for a physical quantum computer use a one-dimensional line of qubits with nearest-neighbor (NN) interactions [1–11], called linear nearest-neighbor (LNN) arrays, where a qubit interacts only with the two qubits adjacent to it. As such, to perform an operation between two remote qubits along the array, that is, between qubits that are not nearest neighbors, often additional SWAP gate operations are required to first bring the qubits adjacent to each other. Since each SWAP gate comprises three CNOT gates [12], the overall computational overhead can be high. Thus, increasing the efficiency of implementing quantum circuits in LNN architectures is an active and important area of research. In fact, it has been shown that if a quantum circuit can be realized efficiently using an LNN architecture, it can be implemented in other architectures as well [13].

The study of efficient realization of quantum circuits on LNN architectures can be broadly classified into two types. The first type of research involves finding methods of translating general quantum circuits into equivalent NN circuits *efficiently*, where worst-case synthesis costs for implementing a general unitary matrix under the NN restriction are investigated. The second type of research, which is the focus of this paper, involves the development of protocols for transmitting quantum states. In any multiqubit quantum system, efficient quantum state transfer is necessary to allow quantum information to be moved around within a quantum processor. In [14], Bose proposed a scheme to use a spin chain as a channel for short-distance quantum communication. Here communication is achieved by encoding a quantum state to be transmitted on a spin at one end of the chain and waiting for a specific amount of time after which the state propagates to the other end. However, due to dispersion of quantum information along the chain, the transport fidelities were less than perfect [14–21]. As a result, several methods of improving the transport fidelity have been investigated. It has been found that perfect transport can be achieved along a spin chain if the nearest-neighbor couplings in the quantum channel are set to very specific values [19,20,22–25]. By encoding the quantum information into low-dispersion wave packets or by encoding or decoding via conditional quantum logic across multiple quantum channels or wires, near perfect transport can be achieved [15,21,26–29]. Other possibilities include using teleportation of the quantum information along the quantum wire by measurements [30], encoding into solitonlike excitations [31], or using quantum cellular automata concepts [32,33]. Besides the transport of single qubits, methods to transport entire qubit registers via quantum mirror wires have also been investigated [24,34–41]. Here an unknown multiqubit quantum state, when encoded at one end of the wire, is transmitted to the other end, in reverse order [34–38], and the process is called mirror inversion (MI). One method of implementing MI processes in spin chains is by pre-engineering spin-spin couplings with a specific pattern. Another method is to repeatedly apply global signal pulses to the system during its dynamical evolution [39–41]. The advantage of such globally controlled MI schemes is that a regular uniformly coupled spin chain can be used, without the necessity to manipulate individual couplings between qubits. Since in some schemes using global control, special block encoding of qubits using additional ancillary qubits is required, the storage density can be less than unity.

*preethika.kumar@wichita.edu

In this paper we present an efficient scheme for quantum state transfer that uses a parity-based MI technique that can be implemented in Ising ($\sigma_Z\sigma_Z$), $\sigma_X\sigma_X$, and $\sigma_Y\sigma_Y$ coupled systems. There are several key features of our scheme. First, we show how to implement a three-qubit parity gate in an Ising coupled system where the gate operation is realized by varying only a single control parameter of the system Hamiltonian. This is achieved by designing the parity gate as a two-control one-target qubit gate. Since the difficulty of implementing our gate is equivalent to that of implementing a CNOT gate in a two-qubit system, for all practical purposes, the parity gate can be considered as an elementary gate. (Under a CNOT gate, the target qubit flips its state from $|0\rangle$ to $|1\rangle$, and vice versa, only if the control qubit is in the $|1\rangle$ state.) Next we show how to use the parity gate to generate efficient circuits for MI as a sequence of controlled-unitary operations between NN qubits. We analytically solve for system parameters for implementing these operations. We next design circuits for implementing MI in $\sigma_X\sigma_X$ and $\sigma_Y\sigma_Y$ coupled systems and analytically show that the same values of the parameters that were calculated for implementing an MI in an Ising coupled system can be used for realizing MI in these systems. That is, using our scheme, MI can be implemented in $\sigma_X\sigma_X$ and $\sigma_Y\sigma_Y$ coupled systems using the same set of parameters for which they can be implemented in an Ising coupled system, without requiring any additional gate operations, which is significant.

Our scheme has several advantages from a practical implementation standpoint. The MI of an N-qubit chain is accomplished in only $N+1$ computational steps (a computational step comprises one or more elementary gates applied in parallel). The scheme is efficient since each computational step is accomplished by varying a single control parameter on all target qubits. The control parameter depends on the physical system under consideration and on the choice of the designer. For instance, when implementing our MI scheme in an Ising coupled system, we choose to vary the biases on individual qubits since they are relatively easy to control. As we will subsequently show, the biases resemble clock pulses and the bias pulses on alternate qubits along an LNN array (with the exception of the first and last qubits) are identical. This symmetry can be used in a practical implementation to reduce the number of control lines, wherein the bias lines for qubits having identical pulse sequences can be tied together. In general, the control circuitry can be reduced to three bias control lines if N is odd and four bias control lines are required if N is even. Another important feature of our scheme is that since every qubit participates in the MI process functioning either as a control or a target, all NN couplings are used. Therefore, we do not need additional measures to cancel the effect of any unwanted interactions, especially in systems with untunable couplings. Also, no additional computational overhead is introduced through the use of additional ancillas for implementing the MI operation nor do we require a pre-engineered Hamiltonian to implement MI.

The paper is organized as follows. In Sec. II we introduce the three-qubit parity gate, which is the basic building block of our MI process. We show how to implement this gate in a three-qubit Ising coupled system by varying only a single parameter of the system Hamiltonian. In Sec. III we show how to construct circuits for implementing MI in N-qubit linear arrays using $N+1$ computational steps. We also show how to extend these circuits to $\sigma_X\sigma_X$ and $\sigma_Y\sigma_Y$ coupled systems by using the same parameters derived for the Ising coupled system. In Sec. IV several applications of MI are presented, which include moving a block of data in one- and two-dimensional (2D) arrays efficiently. In Sec. V the effects of unwanted couplings, parameter mismatches, and rise and fall times on the performance of our MI scheme are discussed. In discussing the effects unwanted couplings, we consider a physical quantum system of superconducting qubits. In Sec. VI we present a summary.

FIG. 1. (a) Two successive CNOT gate operations, which perform the $C^2(\mathbf{P})$ gate operation as given by Eq. (1). For both gates, qubit Q_2 is the target qubit. (b) Our representation of the $C^2(\mathbf{P})$ gate as a single elementary gate operation. Here the vertical line connecting qubits Q_1, Q_2, and Q_3 shows that the gate operation involves all three qubits. To distinguish between the two controls and the target, a square with the letter P is placed on the target qubit. This indicates that after the gate operation, the state of the target qubit Q_2 will hold the parity of the three qubits, while the states of the two-control qubits Q_1 and Q_3 remain unchanged [Eq. (1)].

II. THREE-QUBIT PARITY-BASED MIRROR INVERSION IN AN ISING COUPLED SYSTEM

We define the three-qubit parity gate, which we will represent as $C^2(\mathbf{P})$, as a two-control one-target qubit gate, which computes the parity of three qubits. Under this gate operation, the target qubit inverts its state from $|0\rangle$ to $|1\rangle$ or vice versa, only if the two-control qubits are in opposite states. That is, the linear transformation under the $C^2(\mathbf{P})$ gate can be represented as

$$|q_1,q_2,q_3\rangle \xrightarrow{C^2(\mathbf{P})} |q_1,\, q_1\oplus q_2\oplus q_3,\, q_3\rangle = \begin{cases} |q_1,q_2,q_3\rangle & \text{for} \quad q_1 = q_3 \\ |q_1,q'_2,q_3\rangle & \text{for} \quad \mathrm{q_1} = q'_3. \end{cases} \tag{1}$$

Here $|q_1, q_2, q_3\rangle$ represents a joint state of qubits Q_1, Q_2, and Q_3, which is one of the eight computational basis states $|000\rangle$ through $|111\rangle$. Qubits Q_1 and Q_3 are controls, while qubit Q_2 is the target. Also, q'_2 (q'_3) represents the complement of q_2 (q_3), i.e., if $q_2 = 0$, then $q'_2 = 1$, and vice versa. Note that the $C^2(\mathbf{P})$ gate is equal to two CNOT gates, one each between qubits Q_1 and Q_2 and qubits Q_2 and Q_3, respectively, with qubit Q_2 as the target qubit for both gates [Fig. 1(a)]. However, since in this paper we devise a method of implementing the $C^2(\mathbf{P})$ gate as a single gate by only varying a single control parameter of the system Hamiltonian, without the need to decompose it into two CNOT gates, hereafter we will represent the $C^2(\mathbf{P})$ gate as shown in Fig. 1(b). Here the vertical line connecting qubits Q_1, Q_2, and Q_3 shows that the gate operation involves all three qubits. To distinguish between the two controls and the target, a square with the letter P in placed on the target

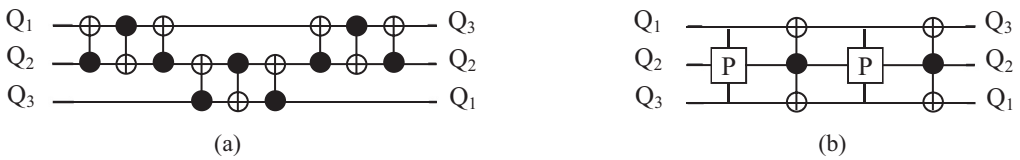

FIG. 2. Swapping the states of qubits Q_1 and Q_3 in a one-dimensional LNN arrangement. (a) Conventional method of using SWAP gates between adjacent qubits, where each swap comprises three CNOT gates. The total gate count of the circuit is 9. Also, since none of the gates can be applied in parallel, the number of computational steps cannot be further reduced by applying gate operations in parallel. (b) Our method of implementing a SWAP operation between qubits Q_1 and Q_3 using the $C^2(\mathbf{P})$ gate instead of SWAP gates. The overall gate count is 6 gates. However, since each pair of CNOT gates following a $C^2(\mathbf{P})$ gate can be applied in parallel, the number of computational steps can be further reduced to 4.

qubit. This indicates that after the gate operation, the state of the target qubit Q_2 will hold the parity of the three qubits, while the states of the two-control qubits Q_1 and Q_3 remain unchanged [Eq. (1)].

We will now show how the $C^2(\mathbf{P})$ gate can be used to perform a MI operation in a three-qubit LNN system where the qubits are arranged along a line in the order Q_1, Q_2, Q_3, with interactions only between qubits Q_1 and Q_2 and between qubits Q_2 and Q_3. There is no interaction between qubits Q_1 and Q_3 and they are called next-to-nearest-neighbor qubits. Note that performing an MI operation in this system is equivalent to swapping the states of the two next-nearest neighbors Q_1 and Q_3. To do so, if we were to use conventional methods of applying successive SWAP gates between adjacent qubits, where each SWAP operation comprises three CNOT gates [12], we would require a total of nine CNOT gates. (Note that when making this comparison we are not considering *XY* coupled and Heisenberg interaction systems, where the natural gate operation is the SWAP.) Figure 2(a) shows the circuit. However, using the $C^2(\mathbf{P})$ gate, we require only a total of six gates as shown in Fig. 2(b): four CNOT and two $C^2(\mathbf{P})$ gates. Moreover, since the two CNOT gates between qubits Q_1 and Q_2 and qubits Q_2 and Q_3 can be applied in parallel, we can combine these two gates into a single computational step, assuming that both CNOT gates require the same time duration. We will hereafter refer to these double CNOT gate operations as the **D** gate operation. Thus, by combining the operation times of gates in parallel, the total number of operations can be further reduced to 4. Observe that the circuit shown in Fig. 2(a) does not have this advantage since none of the gates can be applied in parallel.

The overall linear transformation under the circuit shown in Fig. 2(b) is

$$\begin{aligned}|q_1,q_2,q_3\rangle &\xrightarrow[\text{step 1}]{C^2(\mathbf{P})} |q_1,\ q_1\oplus q_2\oplus q_3,\ q_3\rangle \\ &\xrightarrow[\text{step 2}]{\text{CNOT}} |q_2\oplus q_3,\ q_1\oplus q_2\oplus q_3,\ q_1\oplus q_2\rangle \\ &\xrightarrow[\text{step 3}]{C^2(\mathbf{P})} |q_2\oplus q_3,\ q_2,\ q_1\oplus q_2\rangle \xrightarrow[\text{step 4}]{\text{CNOT}} |q_3,q_2,q_1\rangle.\end{aligned} \tag{2}$$

From Eq. (2) we can see that the states of qubits Q_1 and Q_3 are interchanged. This method of using $C^2(\mathbf{P})$ gates in conjunction with CNOT gates can be extended to implement SWAP operations between arbitrarily separated qubits in NN arrays, as we will show in the next section.

To demonstrate how to implement a $C^2(\mathbf{P})$ gate operation, consider a three-qubit Ising coupled NN system with the Hamiltonian

$$\mathbf{H} = \sum_{i=1}^{3}(\Delta_i\boldsymbol{\sigma}_{\mathbf{X}i} + \varepsilon_i\boldsymbol{\sigma}_{\mathbf{Z}i}) + \xi\sum_{i=1}^{2}\boldsymbol{\sigma}_{\mathbf{Z}i}\boldsymbol{\sigma}_{\mathbf{Z}i+1}. \tag{3}$$

Here ε_i and Δ_i are the bias and tunneling parameters for qubit Q_i, and $\boldsymbol{\sigma}_{\mathbf{X}i}$ and $\boldsymbol{\sigma}_{\mathbf{Z}i}$ for $i = 1, 2, 3$ are the corresponding Pauli spin matrices for each qubit. The nearest-neighbor couplings between qubits Q_1 and Q_2 and qubits Q_2 and Q_3 are assumed to be equal in magnitude ξ and are diagonal in the interaction basis. The Hamiltonian model given by Eq. (3) can be used to represent physical systems with and without tunable couplings [42–44]. For instance, in charge qubits with fixed interactions [43], the coupling between qubits will be a fixed capacitance between adjacent boxes. In a tunable coupling system as in [44], where nearest-neighbor charge qubits are coupled through loop-shaped electrodes with Josephson junctions (JJs) at the loop intersections, the coupling between two qubits is varied by varying the bias current through the Josephson-junction loop.

To implement the $C^2(\mathbf{P})$ gate operation, we use the pulsed bias scheme proposed in [45,46], which is a scheme for implementing controlled-unitary operations. In this scheme, only a single pulse is applied on the target qubit (in this case, Q_2) and no operation is performed on the control qubits (Q_1 and Q_3) [45,46]. The magnitude and the duration of the pulse depend upon the gate operation that is performed and also on whether the system is operating in the weak- ($\xi < \Delta$) [45] or strong- ($\xi_1 > \Delta$) [46] coupling regime. Suppose the couplings are strong. Then, by setting the biases on the two-control qubits to any arbitrary value, including zero, such that it does not cancel the effect of the couplings, we can essentially freeze their dynamics, wherein each qubit only undergoes Z precessions at rates determined by the magnitudes of the couplings [46]. As a result, 2×2 reduced Hamiltonians can be written for the target qubit Q_2 in a subspace $|\psi\rangle$, where $|\psi\rangle$ corresponds to a joint state of qubits Q_1 and Q_3, which is $|00\rangle$, $|01\rangle$, $|10\rangle$, or $|11\rangle$ [46]:

$$\begin{aligned}\mathbf{H}_2^{|\psi\rangle} &= \Delta_2\boldsymbol{\sigma}_{\mathbf{X}} + (\varepsilon_2 + \xi\langle\psi|\boldsymbol{\sigma}_{\mathbf{Z}1}|\psi\rangle + \xi\langle\psi|\boldsymbol{\sigma}_{\mathbf{Z}3}|\psi\rangle)\boldsymbol{\sigma}_{\mathbf{Z}} \\ &\quad + (\varepsilon_1\langle\psi|\boldsymbol{\sigma}_{\mathbf{Z}1}|\psi\rangle + \varepsilon_3\langle\psi|\boldsymbol{\sigma}_{\mathbf{Z}3}|\psi\rangle)\mathbf{I}.\end{aligned} \tag{4}$$

Here the subscript 2 in the Hamiltonian represents qubit Q_2 and $\mathbf{I}$ is the 2×2 identity matrix. Since $|\psi\rangle$ can be one of four states, there are four reduced Hamiltonians for qubit Q_2.

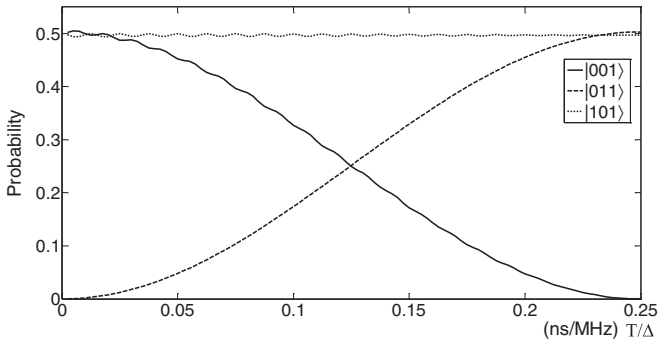

FIG. 3. Simulation results for the $C^2(\mathbf{P})$ gate when the initial state is an equal superposition of the $|001\rangle$ and $|101\rangle$ states, respectively. The plot shows the evolution of probabilities of the different basis states of the system (except for those states whose probabilities remain zero throughout). From the plots we can see that, under the $C^2(\mathbf{P})$ gate, the $|101\rangle$ initial state remains in the same state, while the $|001\rangle$ initial state changes to $|011\rangle$, confirming the $C^2(\mathbf{P})$ gate operation.

Integrating the Hamiltonian using the Schrödinger equation, we obtain the following unitary matrix for the evolution of qubit Q_2 in subspace $|\psi\rangle$:

$$\mathbf{U} = e^{i\theta} \times \begin{pmatrix} \cos(2\pi f t) - \frac{iE}{f}\sin(2\pi f t) & \frac{-i\Delta_2}{f}\sin(2\pi f t) \\ \frac{-i\Delta_2}{f}\sin(2\pi f t) & \cos(2\pi f t) + \frac{iE}{f}\sin(2\pi f t) \end{pmatrix}, \tag{5}$$

where

$$E = \varepsilon_2 + \xi \langle\psi|\boldsymbol{\sigma}_{\mathbf{Z}1}|\psi\rangle + \xi \langle\psi|\boldsymbol{\sigma}_{\mathbf{Z}3}|\psi\rangle, \tag{6}$$

$$f = \sqrt{{\Delta_2}^2 + E^2} \tag{7}$$

and

$$\theta = -2\pi t \left(\varepsilon_1 \langle\psi|\boldsymbol{\sigma}_{\mathbf{Z}1}|\psi\rangle + \varepsilon_3 \langle\psi|\boldsymbol{\sigma}_{\mathbf{Z}3}|\psi\rangle\right). \tag{8}$$

Equation (5) describes the unitary evolution of the target in subspace $|\psi\rangle$. Here we have normalized the Planck constant to 1. Also, by appropriately choosing the values of the biases on Q_1 and Q_3, the phase in a subspace as given by Eq. (8) can be made zero (or an integer multiple of 2π).

Under the $C^2(\mathbf{P})$ gate, we want qubit Q_2 to invert its state when Q_1 and Q_3 are in opposite states. This means that in the $|01\rangle$ or $|10\rangle$ subspaces, we need the effective bias E to be zero, which allows qubit Q_2 to undergo Rabi oscillations between its $|0\rangle$ and $|1\rangle$ states at a rate $2\pi\Delta_2 t$ in these subspaces. From Eq. (6), since the two coupling terms, being equal in magnitude, completely cancel each other in these subspaces, to implement the $C^2(\mathbf{P})$ gate, we simply need to make the bias ε_2 on Q_2 zero, for a time step T such that

$$T = \frac{4P+1}{4\Delta_2}, \tag{9}$$

where P is an integer [45,46]. From Eq. (9), qubit Q_2 undergoes a quarter-cycle oscillation, wherein it inverts its state in the $|01\rangle$ and $|10\rangle$ subspaces. Note that, in the $|00\rangle$ and $|11\rangle$ subspaces, qubit Q_2 only undergoes Z precessions, since the bias ε_2 does not cancel out the effect of the strong couplings. The values of the couplings can be chosen such that these precessions result in identity gate operations on the target qubit in the $|00\rangle$ and $|11\rangle$ subspaces [45,46]. One set of parameters in the strong-coupling regime, which we have used in our simulations, consists of $\Delta_1 = \Delta_2 = \Delta_3 = 25$ MHz, $T = 10$ ns, $\varepsilon_1 = \varepsilon_3 = 3$ GHz, $\xi = 1$ GHz, and $\varepsilon_2 = 0$. (The tunneling parameter is assumed to be fixed at the same magnitude for all qubits, even though methods to tune the tunneling have been experimentally demonstrated [47].) Initially, the bias on target qubit Q_2 is 3 GHz. To implement the gate, the bias on qubit Q_2 is made zero for a time step of $T = 0.25\Delta$ (for $\Delta = 25$ MHz and $T = 10$ ns), after which it is raised to its initial value (3 GHz) once again. Simulations confirmed the gate operation and the average fidelity was 100%. In calculating the average fidelity, simulations were run for each of the eight basis states $|000\rangle$

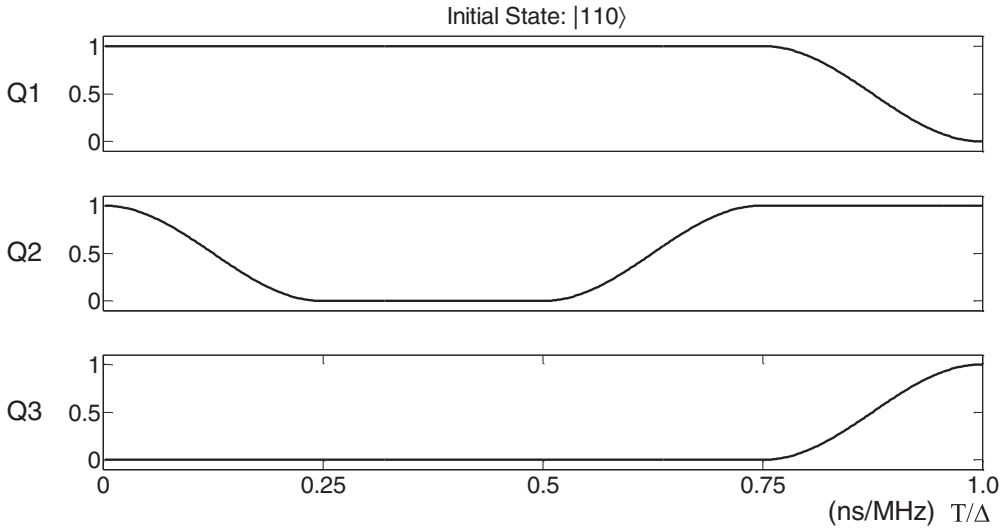

FIG. 4. Simulation results for the MI operation between qubits Q_1 and Q_3 in a three-qubit LNN system using the circuit shown in Fig. 2(b). The initial state of the system is $|110\rangle$, where the probabilities in the $|1\rangle$ state of each qubit has been plotted. The final state is $|011\rangle$, which confirms the SWAP operation between qubits Q_1 and Q_3.

through $|111\rangle$, the fidelity was calculated for each input state, and then an average was computed. The following equation was used to compute the fidelity [12]:

$$F = \mathrm{tr}(\sqrt{\sqrt{\rho}\sigma\sqrt{\rho}}), \tag{10}$$

where σ is the density matrix of the desired state and ρ is the density matrix of the final state obtained after simulation. Figure 3 shows an example of simulation results when the initial state is an equal superposition of the $|001\rangle$ and $|101\rangle$ states, respectively. The plot shows the evolution of probabilities of the different basis states of the system (except for those states whose probabilities remain zero throughout). From the plots we can see that, under the gate operation, the $|101\rangle$ initial state remains in the same state, while the $|001\rangle$ initial state changes to $|011\rangle$, confirming the $C^2(\mathbf{P})$ gate operation.

Next, to implement the MI operation between qubits Q_1 and Q_3, we simulated the circuit shown in Fig. 2(b). Assuming ideal pulses, the simulation was divided into four time steps of duration $T = 0.25\Delta$ (in our simulations, we used $\Delta = 25$ MHz, wherein $T = 10$ ns). When the qubits were idle and no gate operations were performed on them, the bias on the qubits was 3 GHz. The value of the bias was randomly chosen such that $\varepsilon \gg \Delta$. [Simulations have shown that the final state is obtained with high probability (greater than 99% if ε is at least 10Δ). However, the larger the value of the bias, the closer the fidelity of the gate operation is to unity.] The first and third time steps correspond to the $C^2(\mathbf{P})$ gate operations, where the bias on qubit Q_2 is made zero for $T = 0.25\Delta$. The second and fourth time steps correspond to two pairs of CNOT gate operations during which the bias on target qubits Q_1 and Q_3 are each lowered to ξ (which is 1 GHz) for $T = 0.25\Delta$ [45,46], while the bias on the control qubit Q_2 is kept high at 3 GHz. Simulations confirmed the gate operation with fidelity of 99.97%. Figure 4 shows simulation results when the initial state is $|110\rangle$, where the probabilities in the $|1\rangle$ state of each qubit have been plotted. The final state is $|011\rangle$, which confirms the MI operation between qubits Q_1 and Q_3.

III. PARITY-BASED MIRROR INVERSION IN LINEAR CHAINS OF NEAREST-NEIGHBOR QUBITS WITH $N > 3$

We will now show how to construct efficient circuits for MI in LNN arrays using the results of Sec. II. Since we will be primarily using an Ising coupled system in our simulations, throughout this section we compare the performance of our circuits to one that uses successive applications of SWAP gates (three CNOT gates) between adjacent qubits. As we will subsequently show, all the methods presented here can be easily extended to $\boldsymbol{\sigma_X\sigma_X}$ and $\boldsymbol{\sigma_Y\sigma_Y}$ coupled systems, by simply exchanging the magnitudes of the bias and tunneling

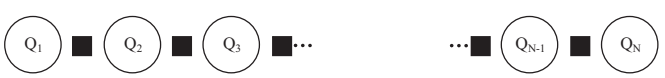

FIG. 5. The LNN arrangement of N qubits (represented as circles) with each qubit coupled only to its immediate neighbors (couplings represented as squares). The couplings may or may not be switchable. Qubits are labeled $Q_1, Q_2, \ldots, Q_N$.

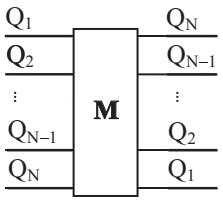

FIG. 6. Symbol for an MI operation, where the states of qubits $Q_1, \ldots, Q_N$ are reversed.

parameters. (Note that even though we do not consider Heisenberg interactions where the natural gate is the SWAP, our scheme can be extended to NN systems with anisotropic Heisenberg interactions when the transverse coupling terms are much smaller than the diagonal coupling terms.)

Consider Fig. 5, which shows a system of N qubits arranged along a one-dimensional array with interactions only between nearest neighbors. The qubits are represented as circles and have been labeled $Q_1, Q_2, \ldots, Q_N$. The couplings have been represented by squares and each qubit only interacts with its nearest neighbors. The couplings may or may not be switchable, depending upon the physical system under consideration. In this system, under an MI, the order of the qubits changes to $Q_N, \ldots, Q_2, Q_1$. Figure 6 shows the symbol that we will use for MI, which comprises a rectangular box with M in it.

We will now introduce four operations that are each constructed using CNOT and $C^2(\mathbf{P})$ gates applied in parallel. All N qubits are involved in these operations, where some of them function as controls and the rest as targets. Each operation corresponds to a single computational step, where we define a computational step as a single operation comprising one or more gates applied *simultaneously* in parallel and within the same time duration. A computational step is analogous to the depth of a circuit, where depth is a measure of the number of layers of gates in a circuit. However, we are using the term computational step since in addition to all gates being applied in parallel, they also are realized within the same time interval. Since we are interested in maximizing the performance of our circuits by lowering both the depth and the quantum cost (number of elementary gates in the circuit), the number of computational steps will be used as a performance measure.

Following are the four operations, the circuit representations for which have been shown in Fig. 7.

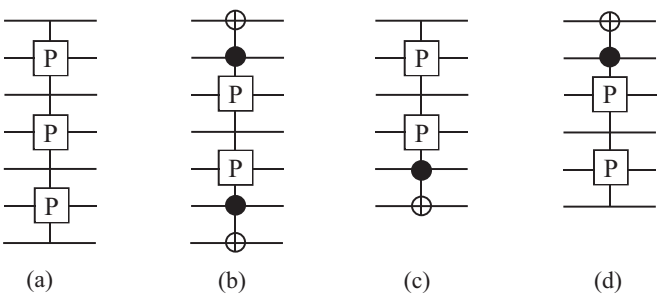

FIG. 7. The (a) P, (b) CNOT-P-CNOT, (c) P-CNOT, and (d) CNOT-P operations.

A. The P operation

We define a P operation as a computational step comprising only of $C^2(\mathbf{P})$ gates applied in parallel. Figure 7(a) shows a P operation for $N = 7$ qubits.

B. The CNOT-P-CNOT operation

We define a CNOT-P-CNOT operation as a computational step comprising $C^2(\mathbf{P})$ gates and two CNOT gates (one at each end of the array) applied in parallel. The CNOT gates are between qubits 1 and 2 and qubits $N-1$ and N, with qubits 1 and N functioning as targets and qubits 2 and $N-1$ functioning as controls. Figure 7(b) shows a CNOT-P-CNOT operation for $N = 7$ qubits.

C. The P-CNOT operation

We define a P-CNOT gate as a computational step comprising $C^2(\mathbf{P})$ gates and one CNOT gate applied in parallel. The CNOT gate is between qubits $N-1$ and N, with qubit N as the target and qubit $N-1$ as the control. Figure 7(c) shows a P-CNOT operation for $N = 6$ qubits.

D. The CNOT-P operation

We define a CNOT-P gate as a computational step comprising $C^2(\mathbf{P})$ gates and one CNOT gate applied in parallel. The CNOT gate is between qubits 1 and 2, with qubit 1 as the target and qubit 2 as the control. Figure 7(d) shows a CNOT-P operation for $N = 6$ qubits.

Each of the four operations shown in Fig. 7 can be implemented by only varying a single control parameter per target qubit. Since the bias on a qubit is relatively easy to control, throughout this paper we will use the bias on individual qubits as our control parameters. Also, as we will shortly show, in our MI scheme, the bias pulses on alternate qubits are identical. Therefore, the bias control lines of alternate qubits along the array can be tied together to a common bias control line. As such, the overall control circuitry can be greatly simplified.

We will now show how each of the four operations shown in Fig. 7 can be used for constructing efficient circuits for MI when $N > 3$. We will first focus on an LNN array such as that shown in Fig. 5 and later extend our scheme to 2D arrays. Using the four operations shown in Fig. 7, we can construct a simple circuit for implementing an MI in only $N+1$ computational steps. Each computational step comprises one of the four operations P, P-CNOT, CNOT-P, and CNOT-P-CNOT. If N is even and $N > 2$, we *alternately* apply the P-CNOT and CNOT-P operations. If N is odd and $N > 3$, we alternately apply the P and CNOT-P-CNOT operations. As examples, Figs. 12(a) and 12(b) show circuits for implementing an MI when $N = 6$ and 7, respectively.

To prove that the circuits in Fig. 8 indeed accomplish MI, we show the equivalence of our circuit to the one presented in [40] by considering a four-qubit system. In [40], the authors showed how to implement MI using a series of controlled-Z and Hadamard (H) gates. Figure 9(a) shows how to implement MI using our scheme. In Fig. 9(b) we replace each of the five P-CNOT and CNOT-P operations by controlled-Z and H gates. Since the H gate is self-inverse, two successive H gates cancel each other and we obtain the reduced circuit shown in Fig. 9(c). Figure 9(d) shows the circuit presented in [40] for MI in a four-qubit system. Note that Figs. 9(c) and 9(d) are equivalent. Figure 9(c) presents the circuit for MI when qubits $Q_1, \ldots, Q_4$ are in arbitrary quantum states. Figure 9(d) presents the circuit for MI when qubit Q_1 is in an arbitrary quantum state, while qubits Q_2, Q_3, and Q_4 are in the $|+\rangle$, $|0\rangle$, and $|+\rangle$ states, respectively. Here the $|+\rangle$ state is the state $(|0\rangle + |1\rangle)/\sqrt{2}$.

To understand how either of the circuits in Fig. 8 works, consider the circuit shown in Fig. 8(a), for $N = 6$ qubits. If $|q_i\rangle$, for $i = 1, \ldots, 6$, is the state of qubit Q_i, the evolution of the states of the six qubits under each of the seven computational steps in Fig. 8(a) is

$$
\begin{aligned}
&|q_1,q_2,q_3,q_4,q_5,q_6\rangle \\
&\xrightarrow{\text{step 1: P-CNOT}} |q_1,\ q_1\oplus q_2\oplus q_3,\ q_3,\ q_3\oplus q_4\oplus q_5,\ q_5,\ q_5\oplus q_6\rangle \\
&\xrightarrow{\text{step 2: CNOT-P}} |q_2\oplus q_3,\ q_1\oplus q_2\oplus q_3,\ q_1\oplus q_2\oplus q_3\oplus q_4\oplus q_5,\ q_3\oplus q_4\oplus q_5,\ q_3\oplus q_4\oplus q_5\oplus q_6,\ q_5\oplus q_6\rangle \\
&\xrightarrow{\text{step 3: P-CNOT}} |q_2\oplus q_3,\ q_2\oplus q_3\oplus q_4\oplus q_5,\ q_1\oplus q_2\oplus q_3\oplus q_4\oplus q_5,\ q_1\oplus q_2\oplus q_3\oplus q_4\oplus q_5\oplus q_6,\ q_3\oplus q_4\oplus q_5\oplus q_6,\ q_3\oplus q_4\rangle \\
&\xrightarrow{\text{step 4: CNOT-P}} |q_4\oplus q_5,\ q_2\oplus q_3\oplus q_4\oplus q_5,\ q_2\oplus q_3\oplus q_4\oplus q_5\oplus q_6,\ q_1\oplus q_2\oplus q_3\oplus q_4\oplus q_5\oplus q_6,\ q_1\oplus q_2\oplus q_3\oplus q_4,\ q_3\oplus q_4\rangle \\
&\xrightarrow{\text{step 5: P-CNOT}} |q_4\oplus q_5,\ q_4\oplus q_5\oplus q_6,\ q_2\oplus q_3\oplus q_4\oplus q_5\oplus q_6,\ q_2\oplus q_3\oplus q_4,\ q_1\oplus q_2\oplus q_3\oplus q_4,\ q_1\oplus q_2\rangle \\
&\xrightarrow{\text{step 6: CNOT-P}} |q_6,\ q_4\oplus q_5\oplus q_6,\ q_4,\ q_2\oplus q_3\oplus q_4,\ q_2,\ q_1\oplus q_2\rangle \\
&\xrightarrow{\text{step 7: P-CNOT}} |q_6,q_5,q_4,q_3,q_2,q_1\rangle\,. \qquad (11)
\end{aligned}
$$

From Eq. (11) we can see that each computational step performs two- or three-qubit exclusive-OR operations between qubits. The qubits that function as controls during a computational step perform as targets in the next computational step. The process of repeatedly applying the P-CNOT and CNOT-P operations in Fig. 8(a) [P and CNOT-P-CNOT operations in Fig. 8(b)] allows us to reverse the order of the qubits in only seven computational steps [eight for Fig. 8(b)]. Likewise, we can show that for any N, the order of the qubits along the array can be reversed in exactly $N+1$ steps. If we use successive applications of SWAP gates between NN qubits, which are used to reverse the order of the qubits, a total of $3(2N-3)$

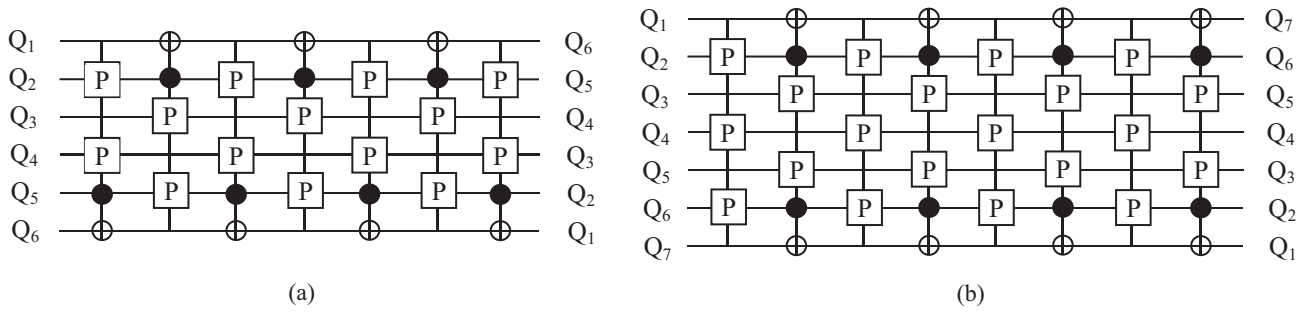

FIG. 8. Circuits for parity-based MI where the order of qubits along an N-dimensional array is completely reversed using only $N+1$ computational steps. If N is even, we alternately apply the P-CNOT and CNOT-P gates. If N is odd, we alternately apply the P and CNOT-P-CNOT gates. (a) Circuit for $N=6$ and (b) circuit for $N=7$. Since all gate operations in a computational step can be simultaneously implemented, the overall circuit complexity and the computational overhead are greatly reduced.

computational steps are required for $N \geqslant 2$ (assuming none of the qubits are ancillas, since a swap between a data qubit and an ancilla requires two CNOT gates). Another significant advantage of the scheme presented here is that in these circuits all N qubits are involved in the gate operations (either as controls or targets). As such, all NN couplings are used in implementing these operations. Thus, the quantum cost and number of computational steps required to implement these operations do not change in systems with untunable couplings because no extra steps are needed to overcome the effects of unwanted NN couplings.

For our simulations, we considered an extension of the three-qubit LNN Ising-coupled Hamiltonian to an N-qubit system

$$\mathbf{H} = \sum_{i=1}^{N} (\Delta \boldsymbol{\sigma}_{\mathbf{X}i} + \varepsilon_i \boldsymbol{\sigma}_{\mathbf{Z}i}) + \xi \sum_{i=1}^{N-1} \boldsymbol{\sigma}_{\mathbf{Z}i} \boldsymbol{\sigma}_{\mathbf{Z}i+1}, \qquad (12)$$

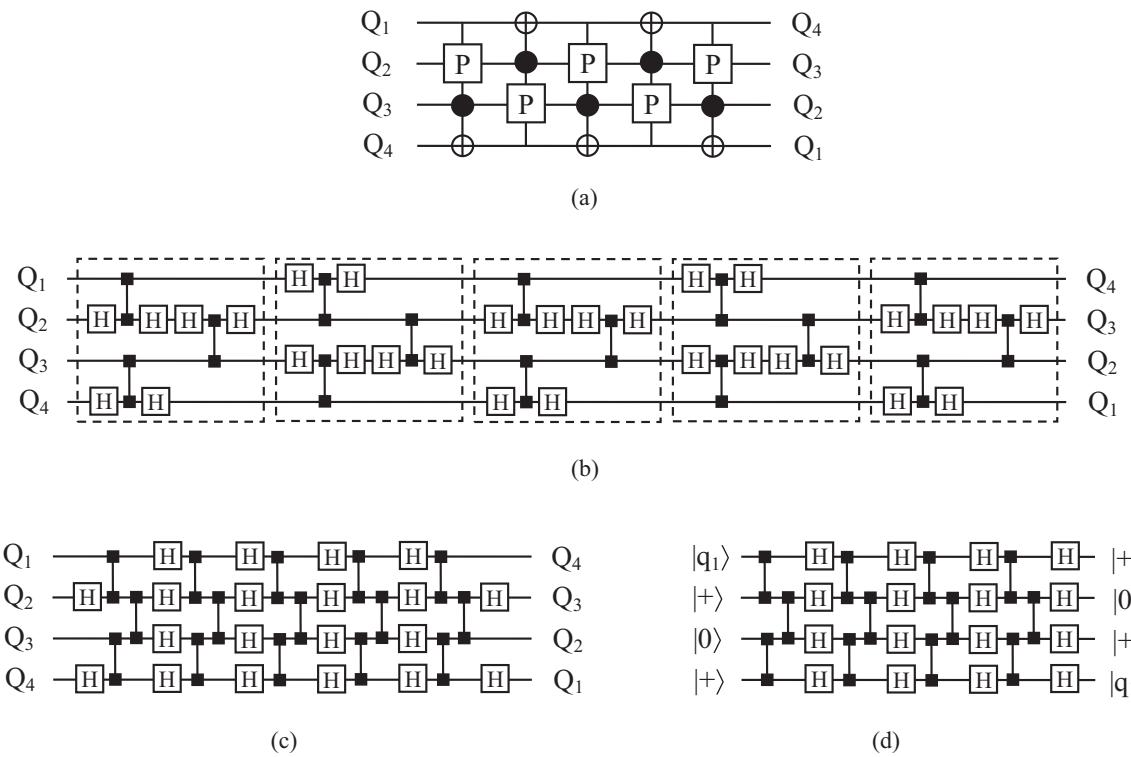

FIG. 9. Equivalence of our circuit with the circuit presented in [40] for MI in a four-qubit system. (a) Circuit for implementing MI using our scheme. (b) Replacing each of the five P-CNOT and CNOT-P operations in (a) by controlled-Z and Hadamard (H) gates. (c) Reduced circuit obtained by canceling two successive H gates (the H gate is self-inverse). (d) Circuit presented in [40] for MI in a four-qubit system. Note that (c) and (d) are equivalent. (c) Circuit for MI when qubits $Q_1, \ldots, Q_4$ are in arbitrary quantum states. (d) Circuit for MI when qubit Q_1 is in an arbitrary quantum state, while qubits Q_2, Q_3, and Q_4 are in the $|+\rangle$, $|0\rangle$, and $|+\rangle$ states, respectively. Here the $|+\rangle$ state is the state $(|0\rangle + |1\rangle)/\sqrt{2}$.

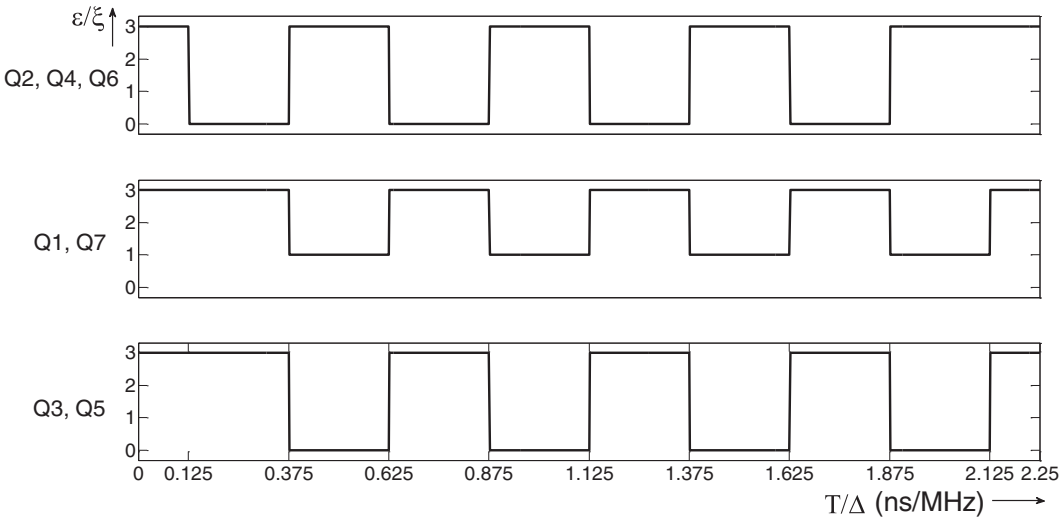

FIG. 10. Sequence of bias pulses on qubits $Q_1, \ldots, Q_7$ under the MI operation. The magnitudes of the bias pulses are in GHz. Also, the first 5 ns and the last 5 ns do not correspond to any gate operation, during which the biases on all seven qubits are maintained at 3 GHz.

where the terms have their usual meaning. The coupling and tunneling parameters were chosen to be the same as those for the three-qubit system ($\xi = 1$ GHz and $\Delta = 25$ MHz). The biases on all qubits were initially kept high at 3 GHz. For a $C^2(\mathbf{P})$ gate, the bias on the target qubit was made zero for 10 ns. For a CNOT gate, the bias on the target qubit was made 1 GHz for 10 ns. Since the gate times of both the CNOT and the $C^2(\mathbf{P})$ gates are the same (10 ns), the duration of each computational step is 10 ns, during which the biases on all target qubits are simultaneously lowered (to either zero or 1 GHz). Figure 10 shows the sequence of bias pulses on a seven-qubit system for implementing the circuit in Fig. 8(b). None of the other parameters of the system were varied ($\xi = 1$ GHz and $\Delta = 25$ MHz). In this system, simulations confirmed the MI operation with an average fidelity of 99.92%. Note that the biases resemble clock pulses and the bias pulses on alternate qubits along the array (with the exception of qubits Q_1 and Q_N) are identical. That is, the bias pulses on qubits Q_2, Q_4, and Q_6 are identical and the bias pulses on qubits Q_3 and Q_5 are identical. When N is odd [as in Fig. 8(b)], the bias pulses on the first and last qubits (here qubits Q_1 and Q_7) are also identical. This symmetry can be used in a practical implementation to reduce the number of control lines, wherein the bias lines for qubits having identical pulse sequences can be tied together. In general, the control circuitry can be reduced to three bias control lines if N is odd and four bias control lines are required if N is even.

Our scheme for MI can be easily extended to $\boldsymbol{\sigma_X\sigma_X}$ and $\boldsymbol{\sigma_Y\sigma_Y}$ coupled systems by using the same parameters derived for an Ising coupled system, with the bias and tunneling terms interchanged (coupling values remain the same as those calculated for an Ising coupled system). To demonstrate, consider the Hamiltonian of a three-qubit $\boldsymbol{\sigma_X\sigma_X}$ coupled system, which is given as

$$\mathbf{H} = \sum_{i=1}^{3} (\Delta_i \boldsymbol{\sigma}_{\mathbf{X}i} + \varepsilon_i \boldsymbol{\sigma}_{\mathbf{Z}i}) + J_X \sum_{i=1}^{2} \boldsymbol{\sigma}_{\mathbf{X}i}\boldsymbol{\sigma}_{\mathbf{X}i+1}, \qquad (13)$$

where, as before, Δ_i and ε_i are the tunneling and bias parameters, respectively, and J_X is the magnitude of the $\boldsymbol{\sigma_X\sigma_X}$ coupling between adjacent qubits. Under the MI operation, the state $|q_1, \ldots, q_N\rangle$ maps to $|q_N, \ldots, q_1\rangle$ for all single-qubit states (not just basis states). Hence, for any single-qubit unitary, we also have that $U^{\otimes N}|q_1, \ldots, q_N\rangle$ maps to $U^{\otimes N}|q_N, \ldots, q_1\rangle$. What this means is that if any Hamiltonian $\mathbf{H_N}$ achieves the MI transformation, so does $U^{\otimes N}\,\mathbf{H_N}\,U^{\dagger\otimes N}$. So, for $\boldsymbol{\sigma_X\sigma_X}$ interactions, we let U be the Hadamard gate, which exchanges the roles of $\boldsymbol{\sigma_X}$ and $\boldsymbol{\sigma_Z}$. This means that the MI operation is accomplished simply by exchanging the control fields for the X and Z magnetic fields. That is, gate operations in the $\boldsymbol{\sigma_X\sigma_X}$ coupled system can be implemented using the *same* parameters for implementing the $C^2(\mathbf{P})$ and $\mathbf{D}$ gates, respectively, in an Ising coupled system, with the parameters Δ_i and ε_i interchanged. The magnitude of the coupling parameters is the same as that solved for under the Ising interactions.

Similarly, for $\boldsymbol{\sigma_Y\sigma_Y}$ interactions, we let $U = (\boldsymbol{\sigma_Y} + \boldsymbol{\sigma_Z})/\sqrt{2}$, which exchanges the roles of $\boldsymbol{\sigma_Y}$ and $\boldsymbol{\sigma_Z}$. That is, the same parameters that accomplish MI in a $\boldsymbol{\sigma_X\sigma_X}$ coupled system can be used to implement MI in a $\boldsymbol{\sigma_Y\sigma_Y}$ coupled system.

IV. APPLICATIONS OF PARITY-BASED MIRROR INVERSION

A. Swapping the states of remote qubits

To swap the states of the first and last qubits along an array, we can apply two MI operations, first between qubits $Q_1, \ldots, Q_N$ and then between qubits $Q_2, \ldots, Q_{N-1}$. The total number of computational steps is $2N$. The number of computational steps can be further reduced from $2N$ to $N + 5$ by dividing the qubits along the array into two groups and then performing MI on each group as shown in Figs. 11(a) and 11(b) when N is even and odd, respectively. Simulations were carried out in a seven-qubit system, which implemented a SWAP operation with an average fidelity of 99.8%. Note that using conventional methods of successively swapping adjacent

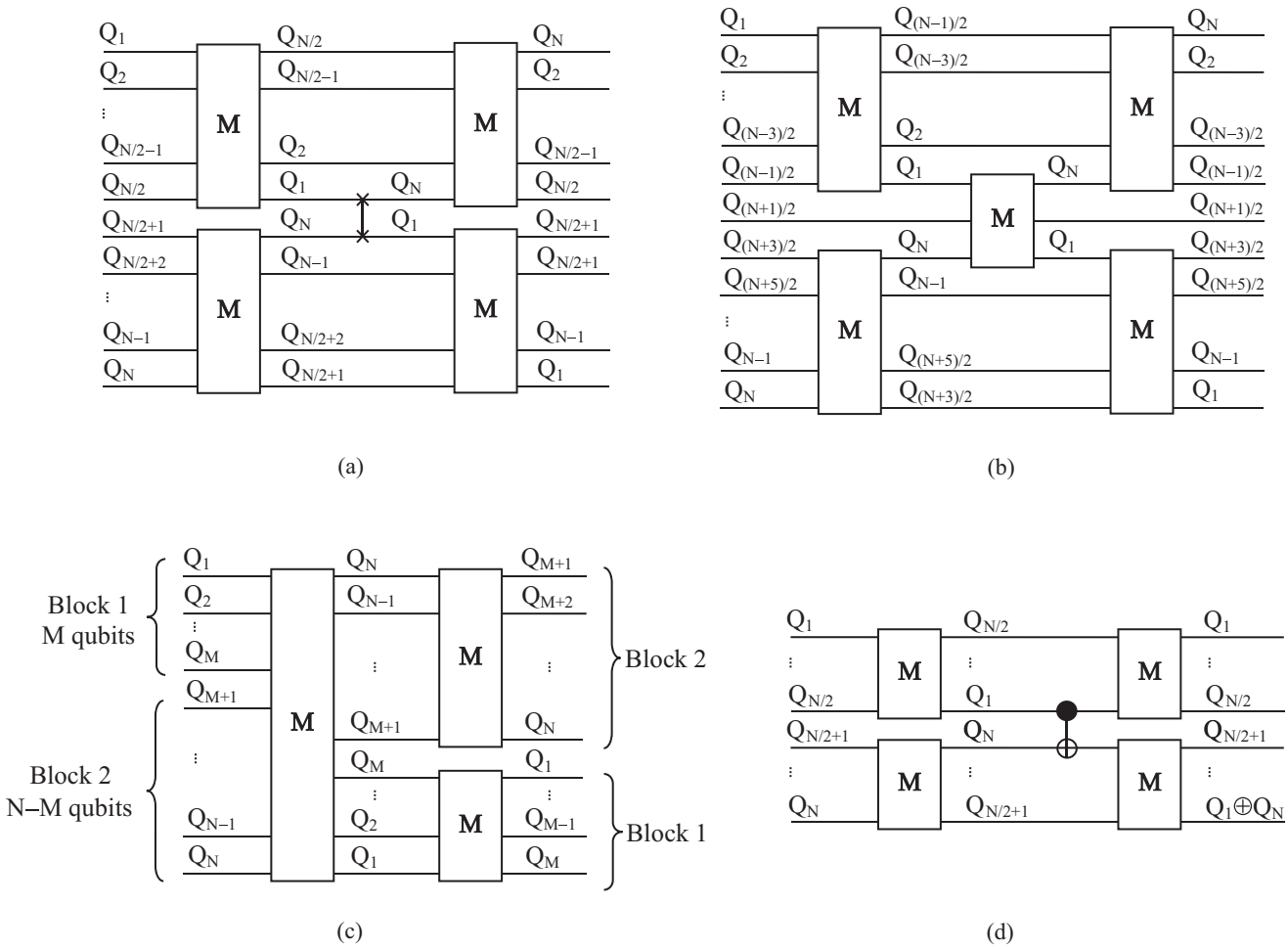

FIG. 11. (a) Circuit for swapping qubits Q_1 and Q_N when N is even. (b) Circuit for swapping qubits Q_1 and Q_N when N is odd. Both circuits require a total of $N+5$ computational steps. In either circuit, the first and last pairs of MIs are applied in parallel. (c) Circuit for moving a block of M qubits in an N-qubit system. The total number of computational steps is $(N+1)+\max\{M+1, N-M+1\}$. The order of the qubits changes $Q_{M+1}, Q_{M+2}, \ldots, Q_N, Q_1, Q_2, \ldots, Q_{M-2}, Q_M$. (d) Circuits for implementing a CNOT gate between remote qubits Q_1 and Q_N. The qubits are divided into two groups and MI is performed on each group in parallel, both before and after the CNOT gate operation.

qubits, a total of $3N$ computational steps is required if N is odd and $N \geqslant 3$ and a total of $3(N-1)$ steps is required when N is even and $N \geqslant 2$.

B. Moving blocks of qubits in LNN arrays

Consider the circuit shown in Fig. 5. Suppose we want to move a block of qubits $Q_1, \ldots, Q_M$, where $M < N$, such that the order of the qubits changes from Q_1, Q_2, $\ldots$, Q_M, $Q_{M+1}, \ldots.., Q_{N-1}, Q_N$ to Q_{M+1}, Q_{M+2}, $\ldots$, $Q_N, Q_1, Q_2, \ldots., Q_{M-2}, Q_M$. That is, the qubits are divided into two blocks on M and $N-M$ qubits and the block of M qubits simply hops over the $N-M$ qubits. Figure 11(c) shows a generalized circuit for achieving this operation using MI. From the figure, the total number of computational steps is $(N+1)+\max\{M+1, N-M+1\}$. (Here $\max\{x, y\}$ gives the maximum of two numbers x and y.) Simulation results for a seven-qubit system confirmed the operation with an average fidelity of 99.76%. Note that if conventional SWAP gates between adjacent qubits are used, $3(N-1)$ computational steps are required.

Moving blocks of qubits will become important in 2D and 3D layouts of qubits, especially in designing quantum memory, where blocks or chains of data will need to be moved around to different locations. Consider Fig. 12(a), which shows a 2D layout of qubits, where qubits are represented by circles and NN couplings between adjacent qubits are represented by dashed lines. In this layout, we are assuming that individual couplings can be switched on and off and a dashed line for the coupling between two qubits means that the coupling is off. A solid line for the coupling between two qubits means that the coupling is on. Suppose we want to move the block or chain of qubits *WXYZ* [black circles in Fig. 12(a)] to the position of the block or chain of qubits *PQRS* (gray circles). For this, first the NN couplings along the chain of qubits *WXYZABPQRS* are switched on [Fig. 12(b)]. Next an MI is performed along the chain so that the order of the qubits now becomes *SRQPBAZXYW* [Fig. 12(c)]. Next the coupling between qubits *A* and *Z* is switched off, which divides the

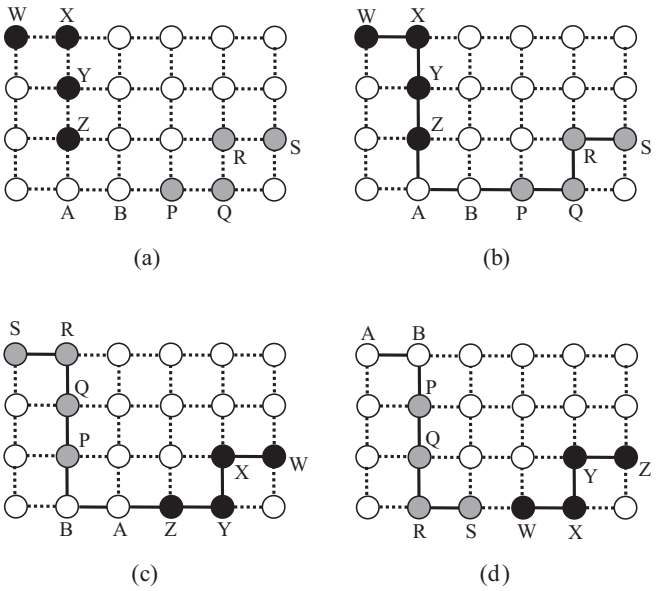

FIG. 12. Moving a block of qubits in a 2D array. Here qubits are represented as circles. Switchable NN couplings are represented as dashed lines and are assumed to be off. Solid lines for the NN couplings indicate that the couplings are on. (a) Suppose we want to move the block or chain of qubits *WXYZ* (black circles) to the position of qubits *PQRS* (gray circles). (b) The NN couplings along the chain of qubits *WXYZABPQRS* is switched on. (c) An MI operation is performed along the chain so that the order of the qubits now becomes *SRQPBAZXYW*. (d) The coupling between qubits *A* and *Z* is switched off, which divides the chain into two chains of six (*SRQPBA*) and four (*ZXYW*) qubits, respectively. An MI operation is performed on each of the two chains, after which qubits *WXYZ* move to the positions of qubits *PQRS*, respectively.

chain into two chains of six (*SRQPBA*) and four (*ZXYW*) qubits, respectively [Fig. 12(d)]. Finally, an MI is performed on each of the two chains, after which qubits *WXYZ* move to the positions of qubits *PQRS*, respectively, as has been shown in Fig. 12(d).

C. Quantum computing between remote qubits

Our MI technique can be used to implement controlled-unitary gate operations between remote qubits in NN architectures. Figure 11(d) shows a method for implementing a CNOT gate between qubits Q_1 and Q_N with qubit Q_1 as the control and Q_N as the target. The circuit requires only $N+3$ computational steps if N is even and $N+4$ steps if N is odd. [Using conventional methods of swapping adjacent qubits, $3N-8$ steps are required if N is even ($N \geqslant 2$) and $3N-5$ steps are required if N is odd ($N \geqslant 5$). In a quantum system, if the only method for bringing remote qubits together to perform a gate operation is by means of SWAP gates, our method will provide a significant improvement in lowering the computational overhead.]

It is important to point out here that all the operations discussed in Secs. II–IV can be easily extended to 2D NN (and possibly 3D NN) layouts. This is because an NN chain of qubits need not be restricted to an LNN array, but can follow a nearest-neighbor 2D (or 3D) path similar to that shown in Fig. 12. Therefore, since all gate operations in Secs. II–IV are designed for a chain of qubits with NN interactions, they can easily be extended to 2D and 3D layouts. Also, several unitary operations can be applied in parallel along the array by dividing the array into two or more NN chains, with no overlap in qubits between the chains.

V. EFFECTS OF UNWANTED COUPLINGS, PARAMETER MISMATCHES, AND FINITE RISE AND FALL TIMES ON GATE OPERATIONS

A. Presence of unwanted couplings

Throughout our discussion, we only assumed couplings between NN qubits. However, in some systems, unwanted couplings might be present that cannot be switched off. For instance, consider Fig. 13,which shows a linear array of three flux qubits [48,49], where each pair of adjacent qubits is coupled through a dc superconducting quantum interference device (SQUID), which makes use of the long-range coupling scheme presented in [50]. The couplings in this system are tunable and can range between positive and negative values.

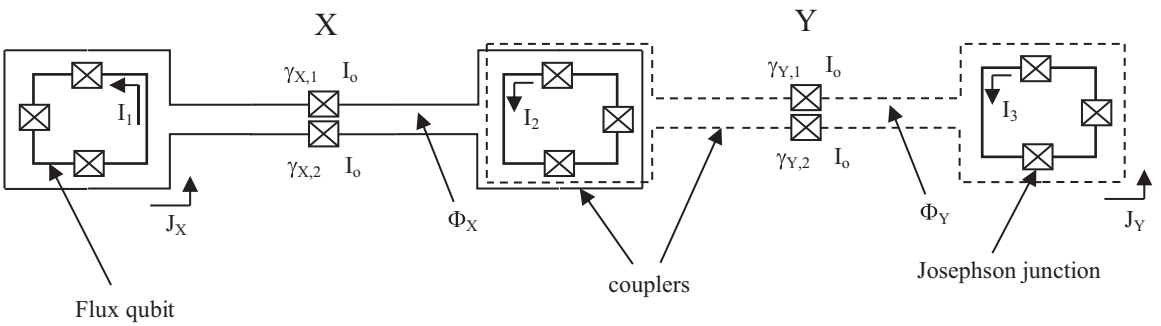

FIG. 13. Linear array of three flux qubits, where each pair of adjacent qubits is coupled through a dc SQUID. Each flux qubit is represented by a square with three JJs (represented as smaller squares with diagonals in them). Larger squares surrounding the qubits and connected through double lines represent couplers between two adjacent qubits. The couplers are labeled *X* and *Y*, where coupler *X* is represented by a solid line and coupler *Y* by a dashed line. The phase difference across the ith junction in coupler n (where $n = X, Y$) is represented by $\gamma_{n,i}$. The applied flux threading through coupler n, its bias current, and its circulating currents are represented by Φ_n, I_n, and J_n, respectively. The critical currents I_o of the JJs in the coupling dc SQUIDs are all assumed to be the same for simplicity.

The couplers are labeled X and Y. We will hereafter use the label n, where $n = X,Y$. The phase difference across the ith junction in coupler n is represented by $\gamma_{n,i}$. The applied flux threading through coupler n, its bias current, and its circulating currents are represented by Φ_n, I_n, and J_n, respectively. The critical current I_o of the JJs in the coupling dc SQUIDs are all assumed to be the same for simplicity. We are able to control the flux independently through each of the coupling dc SQUIDs and the flux qubits.

The total Hamiltonian of the system is given as

$$\mathbf{H} = \sum_{j=1,2,3} \frac{1}{2}(\Delta_j \boldsymbol{\sigma}_{\mathbf{X}_j} + \varepsilon_j \boldsymbol{\sigma}_{\mathbf{Z}_j}) - \sum_{i \neq j} K_{ij} \boldsymbol{\sigma}_{\mathbf{Z}_i} \boldsymbol{\sigma}_{\mathbf{Z}_j}. \quad (14)$$

Here ε_j is the bias energy acting on individual qubits, which depends on the flux threaded through the qubit, and can be independently controlled; Δ_j is the tunneling energy, which can be taken to be fixed during fabrication, even though methods for varying the tunneling have been experimentally demonstrated [47]; and K_{ij} is the coupling energy between qubits i and j and is given as [51,52]

$$K_{ij} = M_{ij} I_i I_j - \sum_{n=X,Y} \sum_{k=X,Y} M_{n,i} M_{k,j} \frac{\partial J_n}{\partial \Phi_k} I_i I_j. \quad (15)$$

Here the first term constitutes the direct coupling between qubits and the other terms constitute the indirect couplings through the dc SQUIDs. Each of the two couplers can be controlled by applying a bias current I_n and/or a bias flux Φ_n. The bias current does not depend on the flux. By adjusting these two parameters the coupling between a pair of qubits can be enhanced or reduced and can be varied between positive and negative values [50]. In our scheme, we can either set the couplings at the start of a computation and treat them as fixed parameters or vary them during the course of a computation. To perform gate operations, the bias on individual qubits can be varied by controlling the flux threading through the qubit.

Note that, in addition to direct coupling between NNs, Eq. (14) also shows an unwanted cross-coupling term K_{13} due to a next-nearest neighbor interaction between qubits 1 and 3. However, as shown in [50], the magnitude of this cross-coupling term is much lower than the direct NN couplings K_{12} or K_{23}. For instance, when K_{12} (or K_{23}) was 1 GHz, K_{13} was found to be around 47 MHz or lower. Moreover, as shown in [50], the effect of the next-nearest-neighbor coupling can be overcome by choosing couplers with longer arm lengths, where the arm length is roughly the distance between two adjacent qubits coupled by a coupler. It was found that the longer the arm length of the coupler, the lower the cross coupling was and for arm lengths greater than 200 μm, the unwanted crosstalk was found to be lower than 5 MHz [50].

To study the effect of this unwanted coupling term on our MI operation, we ran simulations on a three-qubit system with an additional coupling term between qubits 1 and 3, K_{13} (or ξ_{13}), where we used two values for K_{13} (47 and 5 MHz) [50]. Further, to match our parameter values with those in [50], we used the following values in our simulations: $\Delta_j =$ 1 GHz, $K_{12} = K_{23} = 866$ MHz (or, equivalently, $\xi_{12} = \xi_{23} =$ 866 MHz), and $T = 1.25$ ns. These values were obtained by scaling up the values obtained in a weak-coupling regime [53] by multiplying each parameter by a scaling factor of 40. This is because in increasing Δ_j from 25 MHz (value of tunneling solved for in Sec. II and in [53]) to 1 GHz we have increased it 40 times. Note that in scaling the time required for each gate operation (P gate and DCN gate), we used Eq. (9) with $P = 1$. [This is because in Sec. II, for $\Delta_j = 25$ MHz we found T to be 10 ns for $P = 0$ using Eq. (9). Since Eq. (9) is linear, if we increase Δ_j to 1 GHz, T becomes 250 ps, which is a very short pulse. We can use larger values of P to increase the value of T, however, simulations showed that the fidelity of either gate operation is decreased if longer duration pulses are used by increasing P.] For the high value of the bias on control qubits, we used 10 GHz. It was found that the higher the value of the bias, the higher the fidelity of either gate operation was. From our simulations we see that when $K_{13} = 47$ MHz, the average fidelities of the P gate and the DCN gate were found to be 99.47% and 98.18%, respectively. When $K_{13} = 5$ MHz, the average fidelities of the P gate and the DCN gate were found to be 99.47% and 99.74%, respectively. (The average fidelities of the P and DCN gates with $K_{13} = 0$ were 99.47% and 99.73%, respectively.) Note that the cross-coupling term K_{13} affects only the evolution of qubits 1 and 3 with respect to each other. When realizing the P gate, since high biases are applied on qubits 1 and 3 since they behave as control qubits, the presence of K_{13} does not have any significant effect on the fidelity of the P gate. However, during the DCN gate, the biases on both qubits are lowered so that the effect of the cross-coupling term can become significant if it is large enough, resulting in lowering of the gate fidelity. In addition to lowering the fidelity of the DCN gate, the presence of the cross-coupling term introduced unwanted relative phases in the overall MI operation. For instance, when $K_{13} = 5$ MHz, relative phases of 20° and 35°, respectively, were picked up by the $|010\rangle$ (and $|111\rangle$) and $|000\rangle$ (and $|101\rangle$) states.

B. Effect of rise and fall times

Typically, in an experimental system, pulses are nonideal with finite rise and fall times. As a result, the switching process itself might give rise to nonideal gate operations wherein the magnitudes of the probability amplitudes can change depending on the slope of the rise and fall lines. Also, if the initial state of the system is in a superposition of two or more computational basis states, random relative phases may occur in the final state as different phases may be picked up by the different basis states during rise and fall times. In [54], the authors proposed an NN architecture that uses special encoding between pairs of qubits that is immune to random relative phases due to rise and fall times. The change in probability amplitudes can be addressed by decreasing the pulse width of the gate operation (from its original value under an ideal pulse and previously referred to as T) to an adjusted value that takes into account the slope of the rise and fall lines. This new value of the gate time can be found through simulations. For instance, in Fig. 2(b) we found that upon introducing rise and fall times of 1 ns each, the overall fidelity of the SWAP gate reduced to 96.4% (for ideal pulses it was 99.97%). This is because the fidelity of the first and second gates drops to 98.93% and 99.25%, respectively. However, on adjusting the

pulse widths of the $C^2(\mathbf{P})$ and a pair of CNOT gates to 9.3 and 9.8 ns, respectively, the fidelities of these gates increased to 99.93% and 99.55%, respectively. As a result, the overall fidelity of the SWAP gate increased to 98.97%. Likewise, for each of the four operations shown in Fig. 7, we can find ideal pulse widths for a given value of N depending on the slope of the rise and fall lines.

C. Effect of parameter mismatches

Parameter mismatches can be due to fabrication defects or when tuning a control parameter. Since for both the CNOT and $C^2(\mathbf{P})$ gates the time step of the gate operation is proportional to the tunneling parameter [Eq. (9)], any mismatches in the tunneling parameter can be overcome by adjusting the pulse width of the bias pulse on the target qubit. Next, suppose the couplings between NN qubits in Fig. 5 are mismatched and are not all equal to ξ. For instance, suppose the coupling between qubits Q_1 and Q_2 is ξ and the coupling between qubits Q_2 and Q_3 is $\xi+\delta$. In this system, the $C^2(\mathbf{P})$ gate between qubits Q_1, Q_2, and Q_3 can be implemented with high fidelity by applying two consecutive bias pulses of magnitude δ and $-\delta$ on target qubit Q_2. Each pulse is applied for duration T as given by Eq. (9). If, however, $\delta \ll \Delta$, we can implement the $C^2(\mathbf{P})$ gate as before by making the bias on qubit Q_2 zero for time step T. The gate operation thus implemented might not be perfect and the magnitude of the error will depend on the ratio δ/Δ, where the smaller the ratio, the higher the fidelity of the gate operation will be.

VI. CONCLUSION

An efficient scheme for quantum state transfer that uses a parity-based MI technique was presented here. The scheme can be implemented in Ising, $\boldsymbol{\sigma_X\sigma_X}$, and $\boldsymbol{\sigma_Y\sigma_Y}$ coupled systems and we showed how to analytically solve for system parameters to implement the operation in these systems. The key feature of our scheme is a three-qubit parity gate, which we designed as a two-control one-target qubit gate. Since the parity gate operation is implemented by only varying a single control parameter of the system Hamiltonian, the difficulty of implementing this gate is equivalent to that of a CNOT in a two-qubit system and therefore it can be considered as an elementary gate for practical implementations. By applying a sequence of $N+1$ parity-based controlled-unitary operations between NN qubits, where all qubits in an N-qubit chain function either as controls or targets, we reversed the order of all qubits along the array. Using our MI scheme, we also showed how to implement a SWAP gate between two arbitrary remote qubits, move a block of qubits, and implement efficient computing between two remote qubits in nearest-neighbor layouts.

ACKNOWLEDGMENTS

This material was based upon work supported, in part, by the National Science Foundation under Award No. EPS-0903806 and matching support from the State of Kansas through Kansas Technology Enterprise Corporation.

[1] B. E. Kane, Nature (London) **393**, 133 (1998).
[2] L. C. L. Hollenberg, A. S. Dzurak, C. Wellard, A. R. Hamilton, D. J. Reilly, G. J. Milburn, and R. G. Clark, Phys. Rev. B **69**, 113301 (2004).
[3] J. K. Pachos and P. L. Knight, Phys. Rev. Lett. **91**, 107902 (2003).
[4] M. Friesen, P. Rugheimer, D. E. Savage, M. G. Lagally, D. W. van der Weide, R. Joynt, and M. A. Eriksson, Phys. Rev. B **67**, 121301(R) (2003).
[5] T. D. Ladd, J. R. Goldman, F. Yamaguchi, Y. Yamamoto, E. Abe, and K. M. Itoh, Phys. Rev. Lett. **89**, 017901 (2002).
[6] E. Novais and A. H. Castro Neto, Phys. Rev. A **69**, 062312 (2004).
[7] L. Tian and P. Zoller, Phys. Rev. A **68**, 042321 (2003).
[8] S. H. W. van der Ploeg, A. Izmalkov, A. M. van den Brink, U. Hübner, M. Grajcar, E. Il'ichev, H.-G. Meyer, and A. M. Zagoskin, Phys. Rev. Lett. **98**, 057004 (2007).
[9] D. S. Wang, A. G. Fowler, and L. C. L. Hollenberg, Phys. Rev. A **83**, 020302(R) (2011).
[10] R. Stock and D. F. V. James, Phys. Rev. Lett. **102**, 170501 (2009).
[11] K. Yang, S. Zhu, and Z. Wang, Phys. Lett. **20**, 991 (2003).
[12] M. A. Nielsen and I. L. Chuang, *Quantum Computation and Quantum Information* (Cambridge University Press, Cambridge, 2001).
[13] D. Maslov, Phys. Rev. A **76**, 052310 (2007).
[14] S. Bose, Phys. Rev. Lett. **91**, 207901 (2003).
[15] V. Giovannetti and R. Fazio, Phys. Rev. A **71**, 032314 (2005).
[16] V. Subrahmanyam, Phys. Rev. A **69**, 034304 (2004).
[17] M. B. Plenio, J. Hartley, and J. Eisert, New J. Phys. **6**, 36 (2004).
[18] G. De Chiara, D. Rossini, S. Montangero, and R. Fazio, Phys. Rev. A **72**, 012323 (2005).
[19] M. Christandl, N. Datta, A. Ekert, and A. J. Landahl, Phys. Rev. Lett. **92**, 187902 (2004).
[20] M. Christandl, N. Datta, T. C. Dorlas, A. Ekert, A. Kay, and A. J. Landahl, Phys. Rev. A **71**, 032312 (2005).
[21] T. J. Osborne and N. Linden, Phys. Rev. A **69**, 052315 (2004).
[22] G. M. Nikolopoulos, D. Petrosyan, and P. Lambropoulos, J. Phys.: Condens. Matter **16**, 4991 (2004).
[23] M. H. Yung and S. Bose, Phys. Rev. A **71**, 032310 (2005).
[24] P. Karbach and J. Stolze, Phys. Rev. A **72**, 030301 (2005).
[25] Y. Wang, F. Shuang, and H. Rabitz, Phys. Rev. A **84**, 012307 (2011).
[26] H. L. Haselgrove, Phys. Rev. A **72**, 062326 (2005).
[27] D. Burgarth and S. Bose, Phys. Rev. A **71**, 052315 (2005).
[28] D. Burgarth, V. Giovannetti, and S. Bose, J. Phys. A: Math. Gen. **38**, 6793 (2005).
[29] D. Burgarth and S. Bose, New J. Phys. **7**, 135 (2005).
[30] J. P. Barjaktarevic, J. Links, G. Milburn, and R. H. McKenzie, Phys. Rev. Lett. **95**, 230501 (2005).
[31] N. Khaneja and S. J. Glaser, Phys. Rev. A **66**, 060301 (2002).
[32] S. C. Benjamin, Phys. Rev. Lett. **88**, 017904 (2001).
[33] G. K. Brennen and J. E. Williams, Phys. Rev. A **68**, 042311 (2003).
[34] C. Albanese, M. Christandl, N. Datta, and A. Ekert, Phys. Rev. Lett. **93**, 230502 (2004).

[35] T. Shi, Y. Li, Z. Song, and C.-P. Sun, Phys. Rev. A **71**, 032309 (2005).
[36] S. R. Clark, C. M. Alves, and D. Jaksch, New J. Phys. **7**, 124 (2005).
[37] M.-H. Yung, Phys. Rev. A **74**, 030303 (2006).
[38] B. H. Nguyen and V. H. Nguyen, Adv. Nat. Sci.: Nanosci. Nanotechnol. **1**, 025003 (2010).
[39] J. Fitzsimons, L. Xiao, S. C. Benjamin, and J. A. Jones, Phys. Rev. Lett. **99**, 030501 (2007).
[40] J. Fitzsimons and J. Twamley, Phys. Rev. Lett. **97**, 090502 (2006).
[41] R. Raussendorf, Phys. Rev. A **72**, 052301 (2005).
[42] Y. Makhlin, G. Schon, and A. Shnirman, Rev. Mod. Phys. **73**, 357 (2001).
[43] T. Yamamoto, Y. A. Pashkin, O. Astafiev, Y. Nakamura, and J. S. Tsai, Nature (London) **425**, 941 (2003).
[44] J. Lantz, M. Wallquist, V. S. Shumeiko, G. Wendin, Phys. Rev. B **70**, 140507(R) (2004).
[45] P. Kumar and S. R. Skinner, Quantum Inf. Comput. **11**, 300 (2011).
[46] P. Kumar, S. R. Skinner, and S. Daraeizadeh, in *Proceedings of the Fifth International Conference on Quantum Nano and Micro Technologies, Nice, 2011* (IARIA XPS, Red Hook, 2011), p. 28.
[47] A. Fedorov, P. Macha, A. K. Feofanov, C. J. P. M. Harmans, and J. E. Mooij, Phys. Rev. Lett. **106**, 170404 (2011).
[48] T. P. Orlando, J. E. Mooij, L. Tian, C. H. van der Wal, L. S. Levitov, S. Lloyd, and J. J. Mazo, Phys. Rev. B **60**, 15398 (1999).
[49] A. G. Fowler, W. F. Thompson, Z. Yan, A. M. Stephens, B. L. T. Plourde, and F. K. Wilhelm, Phys. Rev. B **76**, 174507 (2007).
[50] P. Groszkowski, A. G. Fowler, F. Motzoi, and F. K. Wilhelm, Phys. Rev. B **84**, 144516 (2011).
[51] J. Ferber and M. Wilhelm, Nanotechnology **21**, 274015 (2010).
[52] I. Serban, E. Solano, and F. K. Wilhelm, Phys. Rev. B **76**, 104510 (2007).
[53] P. Kumar and S. R. Skinner, Phys. Rev. A **76**, 022335 (2007).
[54] P. Kumar, S. R. Skinner, and S. Daraeizadeh, Quantum Inf. Process. **12**, 157 (2013).